



Cite this: DOI: 10.1039/d1sm01774h

## Stimuli-responsive polyelectrolyte surfactant complexes for the reversible control of solution viscosity†

 Giuseppe Rosario Del Sorbo,<sup>ab</sup> Daniel Clemens,<sup>c</sup> Emanuel Schneck<sup>ib</sup>\*<sup>d</sup> and Ingo Hoffmann<sup>ib</sup>\*<sup>b</sup>

Interactions of polyelectrolytes with oppositely charged surfactants can give rise to a large variety of self-assembled structures. Some of these systems cause a drastic increase in solution viscosity, which is related to the surfactant forming aggregates interconnecting several polyelectrolyte chains. For these aggregates to form, the surfactant needs to be sufficiently hydrophobic. Here, we present a system consisting of the anionic surfactant sodium monododecyl phosphate and the cationic cellulose-based polyelectrolyte JR 400. The hydrophobicity of the surfactant can be controlled by the solution's pH. At  $\text{pH} > 12$ , the surfactant headgroup bears two charges. As a consequence, the solution viscosity decreases drastically by up to two orders of magnitude, while it can be as high as 10 Pa s at lower pH. In this paper, we investigate the changes of the mesoscopic structure of the system which lead to such drastic changes in viscosity using small angle neutron scattering and neutron spin-echo spectroscopy. Such systems are potentially interesting as they allow for a modular design where stimuli responsiveness is introduced by relatively small amounts of surfactant reusing the same simple polyelectrolyte.

 Received 15th December 2021,  
 Accepted 2nd March 2022

DOI: 10.1039/d1sm01774h

[rsc.li/soft-matter-journal](https://rsc.li/soft-matter-journal)

## 1 Introduction

Aqueous solutions containing polyelectrolytes (PE) and oppositely charged ionic surfactants have attracted much interest over the last two decades due to their relevance in fundamental polymer- and biophysics but also with regard to their potential applications in pharmaceuticals, engineering, and food sciences.<sup>1–5</sup> The self-assembly of PE-surfactant-complexes (PESCs) starts occurring at the critical aggregation concentration (cac), which is generally lower than the critical micellar concentration (cmc) of the surfactants alone.<sup>3,6,7</sup> The assembly process is controlled by several parameters such as PE charge density<sup>8,9</sup> and stiffness<sup>10</sup> or the surfactant alkyl tail length,<sup>11</sup> among others.

Stoichiometric PESCs with zero net charge are water-insoluble,<sup>12,13</sup> while non-stoichiometric ones with a significant

positive or negative net charge are usually soluble. Depending on their mesoscopic structures, PESCs can be used to tune the rheological properties of aqueous solutions in which they are present. In a recent study on the interaction of the cationic cellulose-based polyelectrolyte JR 400 with anionic alkyl sulphate surfactants of variable alkyl tail length, a dramatic difference in the solution viscosity by 3 orders of magnitude has been demonstrated to originate from the different PE-surfactant mesoscopic organisation.<sup>11</sup> In particular, it was found that high viscosity coincides with the presence of rod-like mixed aggregates that are only formed when the surfactants have long-enough alkyl tails (C12 or C14) and are thus sufficiently hydrophobic, in line with earlier reports on C12 surfactants.<sup>7,10,14,15</sup> These mixed rod-like aggregates act as cross-links connecting different PE chains, imparting viscoelastic properties to the solution with a characteristic increase of viscosity close to the phase boundary on the PE-rich side.<sup>7,14,15</sup> In contrast, no such aggregates and consequently no significant increase in viscosity are observed when alkyl sulphates with shorter tails (C8) are added to aqueous PE solutions.<sup>11</sup>

Like PESC solutions, also worm-like micelle (WLMs) can exhibit viscoelastic behaviour.<sup>16–21</sup> Under certain conditions, WLMs can form an entangled network leading to increased zero-shear viscosity and shear thinning behaviour.<sup>22–24</sup> These supramolecular structures have earned the name smart WLMs since they are able to change their properties in response to

<sup>a</sup> Max Planck Institute of Colloids and Interfaces, Am Mühlenberg 1, D-14476 Potsdam, Germany

<sup>b</sup> Institut Max von Laue-Paul Langevin (ILL), 71 Avenue des Martyrs, CS 20156, F-38042 Grenoble Cedex 9, France. E-mail: hoffmann@ill.fr

<sup>c</sup> Helmholtz-Zentrum Berlin, Hahn-Meitner Platz 1, D-14109, Berlin, Germany

<sup>d</sup> Department of Physics, Technische Universität Darmstadt, Hochschulstraße 8, D-64289 Darmstadt, Germany. E-mail: emanuel.schneck@pkn.tu-darmstadt.de

† Electronic supplementary information (ESI) available: Additional rheology, SANS and NSE measurements as much as a video showing the change in viscosity upon pH adjustment. See DOI: 10.1039/d1sm01774h

external stimuli, such as UV/visible light, temperature changes, or pH variations.<sup>25,26</sup> Similarly, smart polymeric materials have gained enormous interest due to their potential in micro-electromechanical or optical applications, as coatings, or for drug delivery and biosensing.<sup>27,28</sup> A wide range of different stimuli responsive polymers can be synthesised,<sup>29,30</sup> among them the thermoresponsive poly(*N*-isopropylacrylamide) (PNIPAAm)<sup>31–34</sup> which has a lower critical solution temperature (LCST) close to body temperature<sup>28,35,36</sup> making it particularly interesting for drug delivery.

However, smart materials based on either WLMs or polymers alone suffer from distinct disadvantages. Polymeric materials require custom synthesis, while for WLMs relatively high surfactant concentrations, typically in excess of 10 mM,<sup>37</sup> 30 mM,<sup>38,39</sup> 40 mM<sup>40,41</sup> or even 60 mM<sup>42</sup> are used to significantly increase the solution viscosity. While this does not pose a problem as long as standard surfactants, such as hexadecyltrimethylammonium bromide (CTAB), but can become problematic if large quantities of a rather exotic stimuli responsive surfactant are needed. In contrast, PESCs with stimuli-responsive surfactants should offer a possibility to avoid these shortcomings. Viscous PESCs can use polymers that are commercially available in large quantities such as JR 400 (see Fig. 1A). And PESCs based on this polymer have previously been shown to increase the solution viscosity by 2–3 orders of magnitude by adding as little as 2 mM of surfactant.<sup>11,14,43</sup> Finally, surfactants sensitive to external stimuli such as temperature,<sup>44–46</sup> light,<sup>47,48</sup> or pH<sup>49–51</sup> are nowadays available. In principle, they allow to impart their stimuli responsiveness on polymeric systems as demonstrated for pNIPAM microgels and polyelectrolytes with photo sensitive azobenzene-containing surfactants.<sup>52,53</sup> In the present work we use JR 400 (see Fig. 1A) in combination with the pH-sensitive surfactant sodium mono dodecyl phosphate (SDP) (see Fig. 1B).

SDP's ionic groups can be protonated or deprotonated by changing the solution pH, which offers the unique possibility to tune the self-assembly of PESCs. We investigate the changes of the mesoscopic structure and dynamics associated to pH variations at different PE/surfactant charge ratios,  $Z$ , using rheology, small angle neutron scattering (SANS) and neutron spin-echo (NSE) measurements. We find that PESCs with SDP with a single negative charge form mixed rodlike PE/surfactant aggregates, which interconnect on average 3 PE chains, thereby increasing the system's viscosity. These aggregates are dissolved when increasing the pH enough to obtain

SDP with 2 negative charges and consequently the viscosity is reduced.

## 2 Materials and methods

### 2.1 Materials

JR 400 (Dow Chemical, USA, see Fig. 1A) is a cationically modified hydroxyethylcellulose with a molecular weight of about 500 000 g mol<sup>-1</sup> (PDI = 1.85,<sup>54</sup> with a partial molar density in water 1.66 g ml<sup>-1</sup>) and a cationic group on 27% of the glucose units, resulting in 1000 g of PE per mol of positive charges.<sup>55</sup> Its overlap concentration was found to be 0.8 wt%.<sup>56</sup>

SDP (98.5%, see Fig. 1B) was purchased from Sigma-Aldrich and used without further purification. At neutral pH, SDP is present in its hydrogen phosphate form with a single negative charge on its headgroup referred to as SDP<sup>-</sup>. Around pH = 9, a transition from hydrogen phosphate to phosphate with 2 negative charges is observed<sup>57,58</sup> (see Fig. S1, ESI†) which is referred to as SDP<sup>2-</sup>. Samples either had a pH of 7 where the surfactant is present in its hydrogen phosphate form with a single charge (SDP<sup>-</sup>) or at pH of 12, where the surfactant is present as a phosphate with two negative charges (SDP<sup>2-</sup>). The pH of the solutions was adapted by adding appropriate amounts of NaOH (≥98%, Sigma-Aldrich) and controlled by Mettler Toledo pH-meter.

It should also be noted that at neutral pH, a small fraction of the surfactant forms an insoluble salt complex,<sup>59</sup> which gives the solutions a turbid appearance.

Water was taken from a Millipore system while SANS and NSE samples were prepared in D<sub>2</sub>O (99.9% isotopic purity, Sigma-Aldrich). Concentrations were adapted to the higher density of D<sub>2</sub>O so as to keep the molar concentrations identical to the corresponding samples in H<sub>2</sub>O. Samples were prepared and characterised at room temperature unless specified otherwise. PESCs have a JR 400 concentration of 1%, which corresponds to a charge concentration of 10 mM. The surfactant concentration is either given in mM or as the charge ratio  $Z = [\text{PE charges}]/[\text{surfactant charges}]$ , where surfactant charges refers to the species with a single charge.

### 2.2 Small angle neutron scattering (SANS)

SANS measurements were performed on the time-of-flight instrument V16 at Helmholtz-Zentrum Berlin (HZB, Berlin, Germany).<sup>60</sup> To cover a range of the magnitude of the scattering vector  $Q = 4\pi/\lambda \sin(\theta/2)$  from 0.02 to 5 nm<sup>-1</sup>, two configurations were used. For the first configuration, a wavelength band 1.78 Å <  $\lambda$  < 3.75 Å and a sample-to-detector distance of 1.7 m were used while for the second configuration a wavelength band 1.56 Å <  $\lambda$  < 9.22 Å and a sample-to-detector distance of 11 m were used. Data reduction was performed with the software package MantidPlot.<sup>61</sup> For an ensemble of monodisperse, randomly oriented, non interacting particles the coherent scattering intensity is given by  $I(Q) = \phi/V_p P(Q)$ , where  $\phi$  is the volume fraction of particles,  $V_p$  is the volume of an individual particle and  $P(Q)$  is the particle form factor.  $P(Q)$  determines

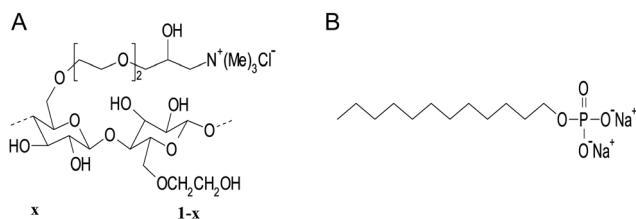


Fig. 1 (A) Chemical structure of JR 400 ( $x = 0.27$ ). (B) Chemical structure of SDP.

the shape of the curve and  $P(Q = 0) = V_p^2 \Delta \text{SLD}^2$ , with the difference in scattering length density between the particles and the solvent  $\Delta \text{SLD}$ . This means that an increase in volume fraction at a given particle size and shape results in an increase in intensity without affecting the shape of the curve, while an increase of the particle size at a given volume fraction increases the intensity and changes the shape of the curve. See the ESI† for details on the data analysis.

### 2.3 Neutron spin-echo spectroscopy (NSE)

Neutron spin-echo spectroscopy (NSE)<sup>62,63</sup> measurements were performed with the instrument IN15<sup>64</sup> at the Institut Laue-Langevin (ILL, Grenoble, France) using 4 different configurations with detector angles  $\theta$  of 7, 4.5, 7.5 and 3.5° using neutrons with wavelengths (longest Fourier time  $t$  in parentheses) of 6 Å (42 ns), 10 Å (190 ns), 10 and 13.5 Å (477 ns) covering a  $Q$ -range from 0.21 to 1.46 nm<sup>-1</sup>. See the ESI† for details on the data analysis.

### 2.4 Rheology

Viscosity measurements were performed using an Anton-Paar MCR 501 Rheometer in cone/plate geometry with a 50 mm cone diameter and 1° cone angle. During the measurements, a solvent trap was used to prevent water evaporation and subsequent changes in the solutions structure. To determine the shear rate dependence, the shear rate was increased from 0.01 s<sup>-1</sup> to 1000 s<sup>-1</sup> and the duration per point was 10 s. Oscillatory shear measurements were performed in the frequency range of 0.01–100 rad s<sup>-1</sup>. The strain amplitude was chosen so as to remain in the linear viscoelastic regime. All measurements were carried out at 25 °C.

## 3 Results and discussion

### 3.1 Rheological behaviour

As already demonstrated for the effect of surfactant chain length,<sup>11</sup> also the charge of the head group plays a crucial role for the macroscopic flow behaviour of PESC. In alkaline solution where the surfactant is double-charged, samples exhibit simple Newtonian behaviour with a viscosity comparable to that of the pure JR 400 solution, while PESC with SDP<sup>-</sup> show a remarkable increase in viscosity. As seen in the flow curves of PE/SDP<sup>-</sup> (see Fig. S3, ESI†), solutions are shear-thinning. Shear-thinning starts at a critical shear rate  $\dot{\gamma}_{\text{crit}}$  which decreases with decreasing  $Z$  (increasing the SDP<sup>-</sup> concentration), similar to what was observed in PESC with JR 400 and SDS or sodium dodecyl benzenesulphonate (SDBS)<sup>7,14</sup> which both have a single negative charge. For JR 400/SDS, it was found that the shear-thinning is related to a slight alignment of mixed PE/surfactant aggregates.<sup>65</sup> The zero-shear viscosity ( $\eta_0$ ) of the system (see Fig. S2, ESI†), increases by 3 orders of magnitude relative to the pure JR 400 solution when adding 5 mM SDP<sup>-</sup> ( $Z = 2$ ) and the structural relaxation time  $\tau_{\text{cross}}$  seen by oscillatory measurements (see Fig. S4, ESI†) increases by 2 orders of magnitude when increasing the surfactant concentration from 1.4 mM to

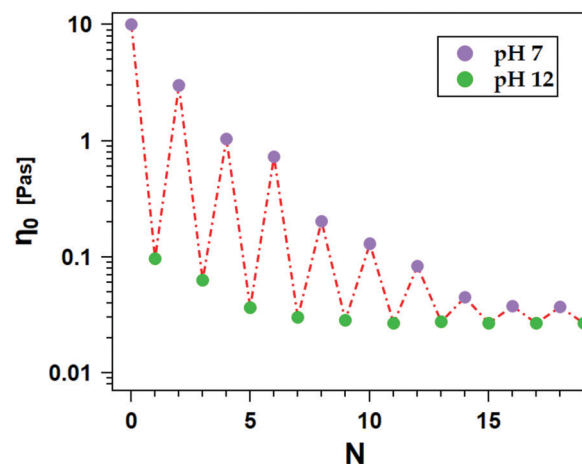


Fig. 2 Zero shear viscosity  $\eta_0$  of SDP as function of the solution pH. Adding either HCl or NaOH the solution pH was changed between 7 and 12 for a certain number of cycles,  $N$ .

5 mM (decreasing  $Z$  from 7 to 2), as found in previous works.<sup>6,15,56,66</sup>

Fig. 2 shows the zero shear viscosity of a sample at  $Z = 3$  where the solution pH was changed back and forth multiple time between 7 and 12 by adding concentrated NaOH or HCl. It is possible to switch between high and low viscosity almost instantaneously (see the video in the ESI†). The switching process can be repeated about 5 times before the viscosity at low pH decreases by a factor 10 relative to the initial solution. This decay is presumably due to a combination of gradual chemical decomposition of the compounds under harsh basic conditions, an increase of ionic strength through the addition of almost 100 mM NaCl (NaOH and HCl) and an increase in aqueous volume by 10%.

### 3.2 Mesoscopic structure and dynamics

Having shown that PESC with SDP can be used as stimuli responsive materials changing the solution viscosity with pH we proceed to elucidate the mesoscopic structure and dynamics of these systems at both high and low pH using small angle neutron scattering (SANS) and neutron spin-echo spectroscopy (NSE).

SANS and NSE measurements on samples with 1% of JR 400 and various surfactant concentrations were performed in order to elucidate the changes in the mesoscopic structure that occur upon pH variation. As in our previous studies<sup>11,14,67</sup> we describe the scattering curve of JR 400 with the form factor of small rods with a radius,  $R_{\text{PE}}$ , of 0.8 nm and a length,  $L_{\text{PE}}$ , of 6 nm. Fig. 3 shows a comparison between the SANS curves of solutions of JR 400/SDP at the same surfactant concentration, namely 5 mM ( $Z = 2$ ) at different pH and the scattering curve of the pure JR 400 solution. It can be seen that at high  $Q$  ( $Q > 0.5 \text{ nm}^{-1}$ ) the scattering curves for pure JR 400 and the PESC at pH 12 where SDP bears 2 negative charges are almost identical while the PESC at pH 7 (SDP<sup>-</sup>) shows a significant increase in scattering intensity, which indicates the formation of structures on a nanometre length scale. The curve shows a slope approximately proportional to  $Q^{-1}$ , indicating that the newly formed

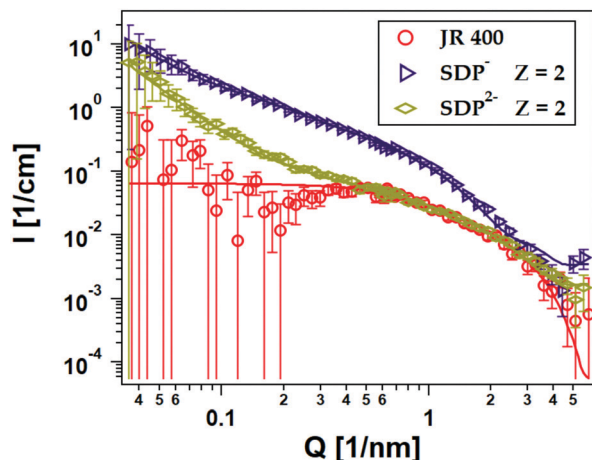


Fig. 3 Comparison of the SANS curves of 1 wt% JR 400 with  $\text{SDP}^-$  and  $\text{SDP}^{2-}$ , both at charge ratio  $Z = 2$  and pure JR 400. While the increase in intensity and the  $Q^{-1}$  slope for the curve of  $\text{SDP}^-/\text{JR 400}$  show the formation of rodlike aggregates, hardly any structural changes compared to the pure PE can be seen for  $\text{SDP}^{2-}/\text{JR 400}$ .

aggregates are cylindrical. At  $Q < 0.5 \text{ nm}^{-1}$  both PESC's show an increase in scattering intensity relative to the pure JR 400 solution, partly because of some insoluble surfactant dimers and partly because of larger clusters.<sup>7</sup> Fig. 4 and Fig. S6 (ESI<sup>†</sup>) show a gradual increase of the high  $Q$  scattering intensity with surfactant concentration without much effect on the shape of the curve, which implies that the extra scattering intensity is due to surfactant aggregates that form at pH 7 but do not significantly change their shape with concentration. At pH 12, the high  $Q$  scattering intensity remains almost unchanged and only at low  $Q$  an increase of the scattering intensity due to the presence of some insoluble surfactant dimers is observed (see Fig. S7, ESI<sup>†</sup>). The fact that there is no change in scattering intensity at high  $Q$  for samples with  $\text{SDP}^{2-}$  means that the

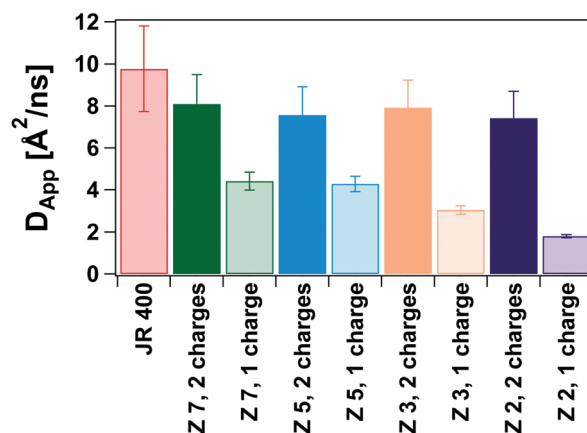
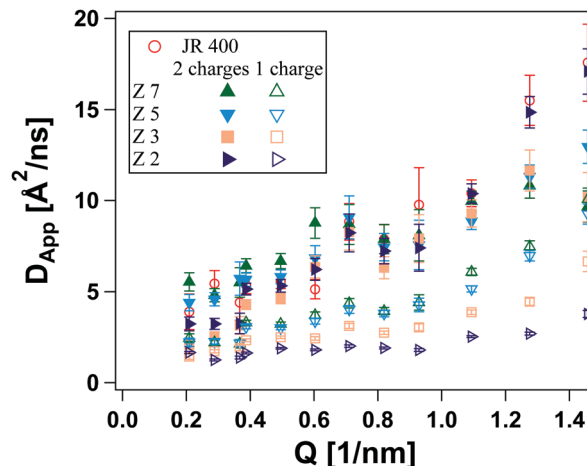


Fig. 5 Top: Apparent diffusion coefficient obtained from fitting eqn (S16) (ESI<sup>†</sup>) to the NSE intermediate scattering functions of pure JR 400 and PESC's with  $\text{SDP}^{2-}$  (closed symbols) and  $\text{SDP}^-$  (open symbols) at different surfactant concentrations; bottom: apparent diffusion coefficient of the same samples at  $Q = 0.93 \text{ nm}^{-1}$ ; while  $\text{SDP}^{2-}$  has only rather little influence on  $D_{\text{app}}$ , addition of  $\text{SDP}^-$  results in the formation of a slower diffusive mode due to the formation of aggregates.

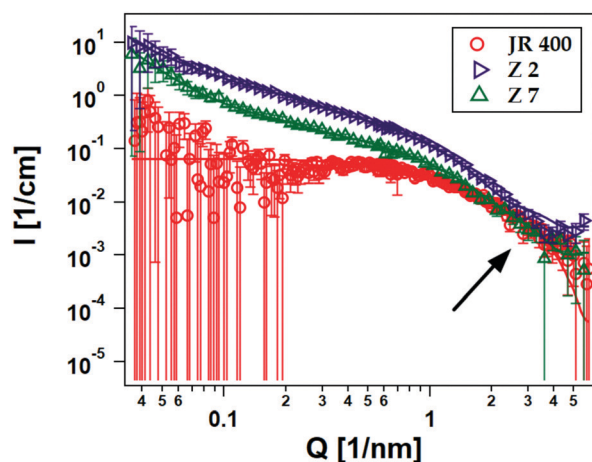


Fig. 4 Comparison of the SANS curves of 1 wt% JR 400 with  $\text{SDP}^-$  at different  $Z$  values and pure JR 400. Raising the surfactant concentration (*i.e.*, reducing  $Z$ ), an increase of the scattering intensity without a change of the shape of the curve is observed at high  $Q$ , because of the formation of mixed aggregates.

double-charged surfactant does not form aggregates and if it absorbs on the PE it only does so in the form of single molecules. The apparent diffusion coefficient  $D_{\text{app}}$  (see Fig. 5) of the pure JR 400 solution determined from NSE shows a linear increase with  $Q$  as expected for a polymer in solution. Addition of  $\text{SDP}^{2-}$  has hardly any effect on  $D_{\text{app}}$  while addition of  $\text{SDP}^-$  results in the emergence of a slow diffusive component at  $Q < 1 \text{ nm}^{-1}$ , due to the surfactant aggregates already observed in SANS. The observations made by SANS and NSE are qualitatively similar to our recent findings for PESC's with JR 400 and either the relatively hydrophobic surfactant sodium tetradecyl sulphate (STS) or the less hydrophobic sodium octyl sulphate (SOS).<sup>11</sup> Therefore, for the PESC's with  $\text{SDP}^-$  which form aggregates, we adopt the fitting procedure that was used there. The kink in the scattering curves at about  $2 \text{ nm}^{-1}$  (see the arrow in Fig. 4) indicates a radius of the cylindrical aggregates of  $R_{\text{agg}} \approx 1.6 \text{ nm}$ , which is similar to that of JR 400/SDS complexes.<sup>14,56,67</sup> All the curves show a strong increase in intensity at  $Q < 0.1 \text{ nm}^{-1}$  due to the presence of both a small

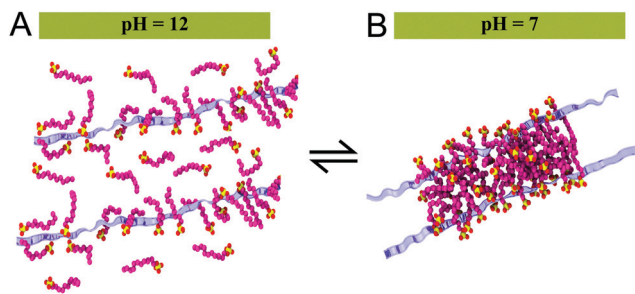


Fig. 6 Schematic description of the pH effect on the SDP/JR 400 solution viscosity. At pH 12 (A) the surfactant bears 2 charges, adsorbing on the PE chains as single molecules. At pH 7 (B) SDP has only a single charge, leading to the formation of mixed, rodlike PE/SDP<sup>-</sup> aggregates which interconnect multiple PE chains.

quantity of non-dissolved material and large scale clusters.<sup>7</sup> The data can be modelled as a superposition of free PE ( $I_{PE}$ ), aggregates ( $I_{agg}$ ) and a power law ( $I_{power}$ ) to take into account the intensity increase at low  $Q$ .

$$I(Q) = I_{agg}(Q) + I_{PE}(Q) + I_{power}(Q) \quad (1)$$

The free PE is modelled as thin cylinder with the same size as found for the pure PE. The macroscopic volume fraction of surfactant in solution,  $\phi_{surf}$ , is not sufficient to account for the volume fraction of the aggregates  $\phi_{agg}$ , meaning that these aggregates consist of both surfactant and PE so that:

$$\phi_{agg} = \phi_{surf} + \phi_{PE}x_{PE} \quad (2)$$

where  $x_{PE}$  represents the fraction of PE incorporated in the aggregates and  $\phi_{PE}$  is the macroscopic PE volume fraction in solution. Accordingly, the volume fraction of free PE reduces to  $\phi_{PE}^{free} = \phi_{PE}(1 - x_{PE})$ , see ESI† for details. From the fits it can be deduced that the aggregates have a radius of  $R_{agg} \approx 1.6$  nm independent of the surfactant concentration. With increasing surfactant concentration more PE is incorporated in the PE/SDP<sup>-</sup> complexes, see Fig. S8 (ESI†). Assuming a homogeneous composition along the long axis of the rodlike aggregates, eqn (S15) (ESI†) can be used to calculate the number of PE chains in an aggregate (see Fig. S8, right axis, ESI†) and it can be seen that the aggregates contain roughly 3 PE chains, so that the aggregates interconnect PE chains and are responsible for the macroscopically observed increase in viscosity, similar to what was found for SDS/JR 400<sup>14</sup> and STS/JR 400.<sup>11</sup> The length of the aggregates cannot be determined from SANS as the power law scattering at low  $Q$  covers the low  $Q$  part of the aggregates from which the length could be deduced. However, this information can be obtained from NSE by identifying the diffusive mode that was observed in samples with SDP<sup>-</sup> as the diffusion of the rodlike aggregates. Modelling of the intermediate scattering function is done as a superposition of rodlike aggregates, free PE and an elastic contribution (see eqn (S26) and Fig. S9–S11, ESI†). The length of the aggregates and the elastic contribution  $S_{el}$  are the only free parameters and the lengths obtained for the aggregates are on the order of 15 nm (see Fig. S12, ESI†). In summary, our investigation of the

mesoscopic structure of SDP/JR 400 PESCs has shown that at pH 12 no aggregates are formed and only a rather small fraction of SDP<sup>2-</sup> is adsorbed on the PE chains as individual molecules (see Fig. 6A) while at pH 7 mixed, rodlike aggregates with radius and length of about 1.6 nm and 15 nm emerge, which cause an increase in viscosity by binding together multiple PE chains as depicted in Fig. 6B.

## 4 Conclusions

In this paper, we have shown that by combining the pH-sensitive surfactant SDP and the polyelectrolyte JR 400 it is possible to control the solution viscosity by adjusting its pH. While hardly any increase in viscosity upon surfactant addition is observed at pH 12, where SDP bears 2 charges, an increase by up to 3 orders of magnitude relative to the pure JR 400 solution is observed at pH 7 where SDP has only a single charge. Using SANS and NSE it is found that the increase in viscosity at pH 7 is due to the formation of mixed, rodlike PE/surfactant aggregates which interconnect approximately 3 PE chains on average. These aggregates are dissolved at pH 12, where the surfactant is less prone to aggregate due to the second head-group charge (see Fig. 6). While the system SDP/JR 400 is of limited practical use due to the relatively small number of times it can be switched back and forth, it nicely demonstrates the feasibility of a modular approach to stimuli responsiveness. The bulk of the system consists of the commercially available PE JR 400, which is not pH-responsive but has a tendency to increase the viscosity of solutions when mixed with small amounts of negatively charged surfactant. The responsiveness comes from a small amount of surfactant which can in principle be exchanged for another surfactant which reacts to another stimulus such as light or temperature, so that it becomes easy to create tailor-made stimuli-responsive solutions.

## Conflicts of interest

There are no conflicts to declare.

## Acknowledgements

Allocation of beamtime by the ILL and HZB is gratefully acknowledged. The raw data of the NSE experiments can be found at [dx.doi.org/10.5291/ILL-DATA.9-12-562](https://dx.doi.org/10.5291/ILL-DATA.9-12-562). G. R. D. S. would like to thank the ILL for support through a PhD scholarship.

## Notes and references

- 1 C. K. Ober and G. Wegner, *Adv. Mater.*, 1997, **9**, 17–31.
- 2 K. J. Crowell and P. M. Macdonald, *J. Phys. Chem. B*, 1997, **101**, 1105–1109.
- 3 D. Langevin, *Adv. Colloid Interface Sci.*, 2009, **147**, 170–177.

- 4 R. A. Campbell, M. Yanez Arteta, A. Angus-Smyth, T. Nylander, B. A. Noskov and I. Varga, *Langmuir*, 2014, **30**, 8664–8674.
- 5 I. S. Oliveira, J. P. Silva, M. J. Araújo, A. C. Gomes and E. F. Marques, *J. Mol. Liq.*, 2021, **322**, 114540.
- 6 M. Tsianou and P. Alexandridis, *Langmuir*, 1999, **15**, 8105–8112.
- 7 I. Hoffmann, M. Simon, B. Farago, R. Schweins, P. Falus, O. Holderer and M. Gradzielski, *J. Chem. Phys.*, 2016, **145**, 124901.
- 8 L. Patel, O. Mansour, M. Crossman and P. Griffiths, *Langmuir*, 2019, **35**, 9233–9238.
- 9 C. Hill, W. Abdullahi, R. Dalglish, M. Crossman and P. Griffiths, *Polymers*, 2021, **13**, 2800.
- 10 L. Chiappisi, I. Hoffmann and M. Gradzielski, *Soft Matter*, 2013, **9**, 3896–3909.
- 11 G. R. Del Sorbo, V. Cristiglio, D. Clemens, I. Hoffmann and E. Schneck, *Macromolecules*, 2021, **54**, 2529–2540.
- 12 B. Lindman, F. Antunes, S. Aidarova, M. Miguel and T. Nylander, *Colloid J.*, 2014, **76**, 585–594.
- 13 H. Wang, Y. Wang, H. Yan, J. Zhang and R. K. Thomas, *Langmuir*, 2006, **22**, 1526–1533.
- 14 I. Hoffmann, B. Farago, R. Schweins, P. Falus, M. Sharp, S. Prévost and M. Gradzielski, *J. Chem. Phys.*, 2015, **143**, 074902.
- 15 I. Hoffmann, P. Heunemann, S. Prévost, R. Schweins, N. J. Wagner and M. Gradzielski, *Langmuir*, 2011, **27**, 4386–4396.
- 16 C. A. Dreiss, *Soft Matter*, 2007, **3**, 956–970.
- 17 M. R. Stukan, E. S. Boek, J. T. Padding, W. J. Briels and J. P. Crawshaw, *Soft Matter*, 2008, **4**, 870–879.
- 18 J. P. Rothstein, *Rheol. Rev.*, 2008, **2008**, 1–46.
- 19 J. F. Berret, in *Molecular Gels, Materials with Self-Assembled Fibrillar Networks*, ed. R. G. Weiss and P. Terech, Springer, Netherlands, 2005, ch. 19, pp. 667–720.
- 20 J. Yang, *Curr. Opin. Colloid Interface Sci.*, 2002, **7**, 276–281.
- 21 S. Candau and R. Oda, *Colloids Surf., A*, 2001, **183**, 5–14.
- 22 Z. Chu, C. A. Dreiss and Y. Feng, *Chem. Soc. Rev.*, 2013, **42**, 7174–7203.
- 23 D. P. Acharya and H. Kunieda, *Adv. Colloid Interface Sci.*, 2006, **123**, 401–413.
- 24 Y. Zhang, Z. Chu, C. A. Dreiss, Y. Wang, C. Fei and Y. Feng, *Soft Matter*, 2013, **9**, 6217–6221.
- 25 A. M. Ketner, R. Kumar, T. S. Davies, P. W. Elder and S. R. Raghavan, *J. Am. Chem. Soc.*, 2007, **129**, 1553–1559.
- 26 X. Liu and N. L. Abbott, *J. Colloid Interface Sci.*, 2009, **339**, 1–18.
- 27 D. W. Löwik, E. Leunissen, M. van Den Heuvel, M. Hansen and J. C. van Hest, *Chem. Soc. Rev.*, 2010, **39**, 3394–3412.
- 28 H. Sun, C. P. Kabb, M. B. Sims and B. S. Sumerlin, *Prog. Polym. Sci.*, 2019, **89**, 61–75.
- 29 S. Tang, PhD thesis, University of Tennessee, 2015.
- 30 D. Wang, Y. Jin, X. Zhu and D. Yan, *Prog. Polym. Sci.*, 2017, **64**, 114–153.
- 31 M. Karg, I. Pastoriza-Santos, L. M. Liz-Marzán and T. Hellweg, *ChemPhysChem*, 2006, **7**, 2298–2301.
- 32 J. Adelsberger, A. Kulkarni, A. Jain, W. Wang, A. M. Bivigou-Koumba, P. Busch, V. Pipich, O. Holderer, T. Hellweg, A. Laschewsky, P. Müller-Buschbaum and C. M. Papadakis, *Macromolecules*, 2010, **43**, 2490–2501.
- 33 H. Kojima, F. Tanaka, C. Scherzinger and W. Richtering, *J. Polym. Sci., Part B: Polym. Phys.*, 2013, **51**, 1100–1111.
- 34 J. E. Wong, A. K. Gaharwar, D. Müller-Schulte, D. Bahadur and W. Richtering, *J. Colloid Interface Sci.*, 2008, **324**, 47–54.
- 35 H. G. Schild, *Prog. Polym. Sci.*, 1992, **17**, 163–249.
- 36 R. Pelton, *Adv. Colloid Interface Sci.*, 2000, **85**, 1–33.
- 37 C. N. Lam, C. Do, Y. Wang, G. Huang and W. Chen, *Phys. Chem. Chem. Phys.*, 2019, **21**, 18346–18351.
- 38 V. Croce, T. Cosgrove, G. Maitland, T. Hughes and G. Karlsson, *Langmuir*, 2003, **19**, 8536–8541.
- 39 M. Calabrese and N. J. Wagner, *ACS Macro Lett.*, 2018, **7**, 614–618.
- 40 B. A. Schubert, N. J. Wagner, E. W. Kaler and S. R. Raghavan, *Langmuir*, 2004, **20**, 3564–3573.
- 41 P. Thareja, I. H. Hoffmann, M. W. Liberatore, M. E. Helgeson, Y. T. Hu, M. Gradzielski and N. J. Wagner, *J. Rheol.*, 2011, **55**, 1375–1397.
- 42 S. R. Raghavan and E. W. Kaler, *Langmuir*, 2001, **17**, 300–306.
- 43 E. Goddard and R. Hannan, *J. Colloid Interface Sci.*, 1976, **55**, 73–79.
- 44 U. Olsson, K. Shinoda and B. Lindman, *J. Phys. Chem.*, 1986, **90**, 4083–4088.
- 45 R. Strey, *Ber. Bunsengesellschaft Phys. Chem.*, 1996, **100**, 182–189.
- 46 O. Glatter, G. Fritz, H. Lindner, J. Brunner-Popela, R. Mittelbach, R. Strey and S. U. Egelhaaf, *Langmuir*, 2000, **16**, 8692–8701.
- 47 M. Umlandt, D. Feldmann, E. Schneck, S. A. Santer and M. Bekir, *Langmuir*, 2020, **36**, 14009–14018.
- 48 S. Chen, R. Costil, F. K. Leung and B. L. Feringa, *Angew. Chem., Int. Ed.*, 2021, **60**, 11604–11627.
- 49 R. Beck, M. Gradzielski, K. Horbaschek, S. S. Shah, H. Hoffmann and P. Strunz, *J. Colloid Interface Sci.*, 2000, **221**, 200–209.
- 50 W. Wang, W. Lu and L. Jiang, *J. Phys. Chem. B*, 2008, **112**, 1409–1413.
- 51 L. Chiappisi, M. Simon and M. Gradzielski, *ACS Appl. Mater. Interfaces*, 2015, **7**, 6139–6145.
- 52 Y. Zakrevskyy, M. Richter, S. Zakrevska, N. Lomadze, R. von Klitzing and S. Santer, *Adv. Funct. Mater.*, 2012, **22**, 5000–5009.
- 53 Y. Zakrevskyy, P. Cywinski, M. Cywinska, J. Paasche, N. Lomadze, O. Reich, H. Löhmannsröben and S. Santer, *J. Chem. Phys.*, 2014, **140**, 044907.
- 54 D. Li, M. S. Kelkar and N. J. Wagner, *Langmuir*, 2012, **28**, 10348–10362.
- 55 K. Thuresson, S. Nilsson and B. Lindman, *Langmuir*, 1996, **12**, 530–537.
- 56 I. Hoffmann, S. Prévost, M. Medebach, S. Rogers, N. Wagner and M. Gradzielski, *Tenside, Surfactants, Deterg.*, 2011, **48**, 488–494.
- 57 K. Nakayama, I. Tari, M. Sakai, Y. Murata and G. Sugihara, *J. Oleo Sci.*, 2004, **53**, 247–265.

- 58 P. Walde, M. Wessicken, U. Rädler, N. Berclaz, K. Conde-Frieboes and P. L. Luisi, *J. Phys. Chem. B*, 1997, **101**, 7390–7397.
- 59 J. Arakawa and B. A. Pethica, *J. Colloid Interface Sci.*, 1980, **75**, 441–450.
- 60 K. Vogtt, M. Siebenbürger, D. Clemens, C. Rabe, P. Lindner, M. Russina, M. Fromme, F. Mezei and M. Ballauff, *J. Appl. Crystallogr.*, 2014, **47**, 237–244.
- 61 O. Arnold, J. C. Bilheux, J. M. Borreguero, A. Buts, S. I. Campbell, L. Chapon, M. Doucet, N. Draper, R. F. Leal, M. A. Gigg, V. E. Lynch, A. Markvardsen, D. J. Mikkelsen, R. L. Mikkelsen, R. Miller, K. Palmen, P. Parker, G. Passos, T. G. Perring, P. F. Peterson, S. Ren, M. A. Reuter, A. T. Savici, J. W. Taylor, R. J. Taylor, R. Tolchenoy, W. Zhou and J. Zikoysky, *Nucl. Instrum. Methods Phys. Res., Sect. A*, 2014, **764**, 156–166.
- 62 F. Mezei, *Z. Phys. A*, 1972, **255**, 146–160.
- 63 *Neutron Spin Echo*, ed. F. Mezei, Springer, Berlin, Heidelberg, 1980, vol. 128.
- 64 B. Farago, P. Falus, I. Hoffmann, M. Gradzielski, F. Thomas and C. Gomez, *Neutron News*, 2015, **26**, 15–17.
- 65 G. R. Del Sorbo, S. Prévost, E. Schneck, M. Gradzielski and I. Hoffmann, *J. Phys. Chem. B*, 2020, **124**, 909–913.
- 66 U. Kästner, H. Hoffmann, R. Donges and R. Ehrler, *Colloids Surf., A*, 1996, **112**, 209–225.
- 67 I. Hoffmann, B. Farago, R. Schweins, P. Falus, M. Sharp and M. Gradzielski, *Europhys. Lett.*, 2013, **104**, 28001.